Applied Physics A manuscript No.
(will be inserted by the editor)

The model oxidation catalyst α-V_2O_5: Insights from contactless in situ microwave permittivity and conductivity measurements

Christian Heine[1], **Frank Girgsdies**[1], **Annette Trunschke**[1], **Robert Schlögl**[1], **Maik Eichelbaum**[1]

Department of Inorganic Chemistry, Fritz-Haber-Institut der Max-Planck-Gesellschaft, Faradayweg 4-6, 14195 Berlin, Germany.

Received: date / Revised version: date

Abstract The in situ microwave cavity perturbation technique was used to study the complex permittivity and conductivity of polycrystalline α-V_2O_5 in a tubular reactor under reactive high temperature conditions with a TM_{110} cavity resonating at 9.2 GHz. The sample was investigated at 400°C in flowing air and air/n-butane mixtures while simultaneously measuring the total oxidation products CO and CO_2 by gas chromatography. The V_2O_5 powder was identified as n-type semiconductor and the dynamic microwave conductivity correlated well with the near-infrared (NIR) absorption assigned to $V3d^1$ band gap states. Correlations between catalytic performance, real and imaginary part of the permittivity and NIR absorption allowed the differentiation between bulk and surface contributions to the charge transport in reactive atmospheres. The stability of the crystalline bulk phase was proven by in situ powder X-ray diffractometry for all applied testing conditions.

Correspondence to: Maik Eichelbaum

Fritz-Haber-Institut der Max-Planck-Gesellschaft

Department of Inorganic Chemistry

Faradayweg 4-6

14195 Berlin, Germany

e-mail: me@fhi-berlin.mpg.de

Fax: +49-30-84134401

Key words complex permittivity, microwave conductivity, heterogeneous catalysis, in situ spectroscopy, solid/gas interface, vanadium oxide

1 Introduction

The interaction between the electronic structure of semiconducting solids and the surrounding gas atmosphere due to chemisorption of gas molecules at the solid surface has for a long time been studied by electrical conductivity measurements [1]. Charge transfer at the solid/gas

interface can significantly affect the charge carrier concentration in the conduction or valence band of a semiconducting solid, and thus its overall conductivity. This observation has found broad applications in the field of gas sensors. However, the same underlying mechanisms play a major role in heterogeneously catalyzed reactions, if reducible solids (such as many transition metal oxides) are at least part of the catalytically active phase [2, 3]. One prominent and industrially highly important class of reactions is the partial oxidation of alkanes to olefins and oxygenates requiring the transfer of a rather high number of charge carriers between catalyst and organic substrate [4]. The direct functionalization of light alkanes is in particular important in light of the upcoming raw material change in the dawning post-crude oil age. An already industrially applied example is the oxidation of n-butane to maleic anhydride, which is produced in a megaton per year range, at about 400°C on vanadyl pyrophosphate [5]. Vanadyl groups (V=O), either in monomeric or polymeric form, are discussed as redox-active species in the catalytic oxidation processes [6]. Hence binary vanadium oxides are highly interesting and structurally well-defined reference materials in order to understand fundamental principles, e.g. the influence of the electronic structure and of charge transfer properties on the catalytic performance [3].

However, 2-contact type electrical conductivity measurements often applied in catalytic in situ experiments are unfortunately rather undefined and provide many sources of error in reactive atmospheres. In particular, erratic contact resistances [7] between electrode and powder and between catalyst grains and particles, possibly even changing under reactive conditions due to water evaporation, catalyst sintering, electrode corrosion, etc., hamper the accurate determination of absolute conductivities and relative changes needed for a rigorous and quantitative correlation of charge transport and catalytic properties.

In order to avoid most of such electrode contact-related problems the microwave cavity perturbation technique (MCPT) has been applied to measure the conductivity and permittivity of powder catalysts under reaction conditions in a contact free manner [8, 9]. Measurements at microwave frequencies have in addition the advantage of probing localized charge transfer processes being in particular important in catalytic reactions, whereas direct current (DC) or low frequency alternating current (AC) methods need macroscopic percolation paths to observe charge transport. In this paper we report on the application of MCPT to the in situ investigation of the complex permittivity and conductivity of vanadium(V) oxide powder under reactive catalytic n-butane oxidation conditions. The tests were run in air and in a reaction feed containing 1 vol% n-butane and 20 vol% oxygen at 400°C. This way, a direct comparison between the conductivity of the highly selective commercial VPP catalyst [10] and the total oxidation (i.e. unselective) catalyst α-V_2O_5 can be made. The results

are explained in the context of further complementary in situ UV/Vis spectrocopy and in situ X-ray powder diffraction (XRPD) experiments under comparable reaction conditions.

2 Experimental

2.1 Sample

The sample under investigation was extra pure α-V_2O_5 powder from Riedel-de Haën. The phase purity was tested by X-ray powder diffractometry (XRPD). The Rietveld analysis of the XRPD pattern shown in Figure 1, exhibits that the α-V_2O_5 powder is phase-pure. The crystal density of the V_2O_5 powder determined from the Rietveld analysis was 3.365 g/cm^3.

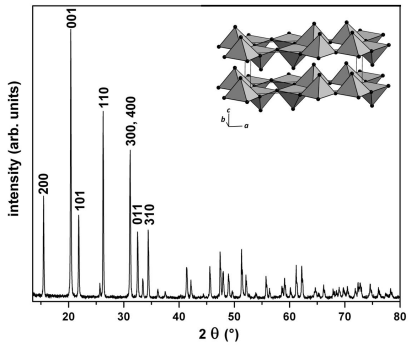

Fig. 1 X-ray powder diffractogram of α-V_2O_5 powder measured at room temperature (most prominent reflections indexed) and representative excerpt of the layered α-V_2O_5 crystal structure with vanadium coordination polyhedra.

2.2 Microwave cavity perturbation measurement

The microwave conductivity setup is illustrated in Figure 2. The microwave cavity (silver-plated brass X-band cavity from ZWG Adlershof) was used in a reflection configuration. One port of the vector network analyzer (Agilent PNA-L N5230C) was connected to the cavity by a coaxial cable and a waveguide. The microwave was coupled from the coaxial cable into the waveguide by an antenna. The coupling between the waveguide and the cavity was realized by an iris, consisting of an aperture and a coupling screw. The coupling screw is made of teflon with a brass tip. For the experiments the TM_{110} mode of the cylindrical cavity was used. The resonance frequency of the loaded and unloaded cavity was in the scan range from 9.21385 GHz to 9.26721 GHz. The scan step size was set to $4 \cdot 10^{-6}$ GHz. The complex reflection factor $\widetilde{\Gamma}(\omega)$, its amplitude being equal to the S_{11} parameter, was detected by the vector network analyzer.

The fixed-bed reactor for catalytic measurements consisted of a 4 mm outer diameter quartz tube located between the two maxima of the electric field. It was connected to a gas supply (mass flow controller manifold) and a gas analytics system (gas chromatograph Agilent 7890). Preheated nitrogen flowing around the reactor was used to heat the sample. The temperature was measured with a K-type thermocouple just outside the cavity. The reactor was surrounded by a vacuum pumped quartz dewar to protect the cavity from convec-

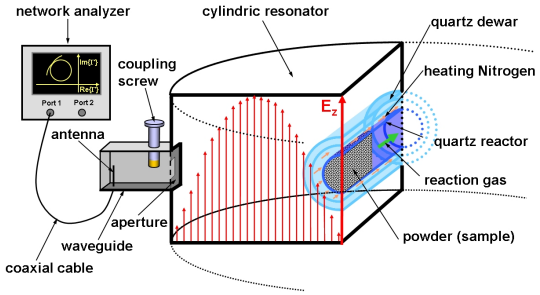

Fig. 2 Schematic presentation of the experimental setup including the network analyzer as microwave source and detector, coupling elements, the microwave cavity, the catalytic quartz reactor with sample position and the double-walled quartz dewar vessel to protect the cavity from convection heat from the reactor.

tion heat. Additionally, the cavity was water-cooled and purged with dry air in order to avoid any effects of air humidity. A detailed description of the heating and gas delivery system was reported previously [8]. This setup offers the possibility to measure the complex permittivity of single crystal and powder samples as a function of time, gas atmosphere, and temperature.

2.3 Catalytic measurements

As for the catalytic and permittivity measurements run in the MCPT setup, the α-V_2O_5 powder was first pelletized, then crushed and sieved. For all measurements shown the sieve fraction between 100 μm to 200 μm was used. The quartz tube reactor with an inner diameter of 3 mm was filled with 71.8 mg of the sieved α-V_2O_5 powder and fixed between two small quartz wool plugs. The catalyst bed length was 10.5 mm corresponding to a powder density of 0.97 g/cm^3. Accordingly, the volume fraction factor f, which is computed from the ratio of the powder and crystal density, was 0.28. The sample was heated to 400°C with a heating rate of 10 K/min in a gas atmosphere of 20 vol% oxygen and 80 vol% nitrogen. After reaching 400°C the catalytic and permittivity data acquisition was started. The sample was kept for 110 min in 20 vol% oxygen and 80 vol% nitrogen. Afterwards, the gas atmosphere was changed to 1 vol% n-butane, 20 vol% oxygen, and 79 vol% nitrogen. After 115 min the mixture was re-seted to 20 vol% oxygen and 80 vol% nitrogen for 235 min. The total gas flow was always 20 ml/min. In the described experiment the complex reflection factor as a function of frequency was measured every 5 min and a gas chromatogram was taken every 20 min.

2.4 In situ X-ray powder diffraction (XRPD)

Ex situ diffractograms were recorded on a Bruker AXS D8 diffractometer. In situ XRPD data were collected on a STOE theta-theta X-ray diffractometer (CuK$\alpha_{1,2}$ radiation, secondary graphite monochromator, scintillation counter) equipped with an Anton Paar XRK 900 high temperature reactor chamber with gas dosing system and coupled Pfeiffer OmniStar quadrupole mass spectrometer to monitor the downstream gas composition. The total flow rate was 100 ml/min. The sample was heated to 400°C with a heating rate of 10 K/min in 20 vol% oxygen and 80 vol% helium. At 400°C it was

kept in this atmosphere for 6.5 hours. Then the gas composition was changed to 1 vol% n-butane, 20 vol% oxygen, and 79 vol% helium for 40 hours. Subsequently, the intial gas atmosphere (20 vol% oxygen and 80 vol% helium) was re-applied for 55 hours. All XRPD data were analyzed by full pattern fitting according to the Rietveld method using the program TOPAS [TOPAS version 3, copyright 1999, 2000 Bruker AXS].

2.5 In situ UV-VIS spectroscopy

The in situ UV-VIS experiment was performed with a Perkin Elmer Lambda 650 spectrometer equipped with a Harrick in situ reaction cell. The UV-VIS spectra were measured in diffuse reflectance geometry from 800 nm (1.55 eV) to 200 mn (6.2 eV) with a stepsize of 1 nm. Every 5 min a spectrum was taken. The Kubelka Munk theory [11] was used to evaluate the data:

$$K/S = \frac{(1-R)^2}{2\ R}, \tag{1}$$

where K is the coefficient of absorption, S the coefficient of scattering, and R the measured reflectance.

α-V_2O_5 powder was heated to 400°C with a rate of 10 K/min in 20 vol% oxygen and 80 vol% helium. At 400°C the sample was kept for 110 min in this gas mixture. Afterwards, the atmosphere was changed to 1 vol% n-butane, 20 vol% oxygen, and 79 vol% helium for 110 min, followed by the re-application of the first mixture for 110 min. The total flow was always 20 ml/min. The CO_2 concentration was detected with a Varian CP-4900 micro gas chromatograph to monitor the catalytic performance of the sample.

3 Results and discussion

3.1 Microwave permittivity and conductivity of α-vanadium(V) oxide

The introduction of a sample into a resonant cavity leads to a shift of the angular resonance frequency ω_0 and a change of the quality factor Q. The quality factor is defined in terms of the maximum stored energy W_s and the average dissipated power P_d in the cavity at the resonance frequency. It can also be expressed as the ratio of the resonance frequency and the full width at half minimum (FWHM) $\Delta\omega$ of the power peak:

$$Q = \left[\omega \frac{W_s}{P_d}\right]_{\omega=\omega_0} = \frac{\omega_0}{\Delta\omega} \tag{2}$$

In the depolarization regime the real part $\epsilon_{1,p}$ and imaginary part $\epsilon_{2,p}$ of the complex powder permittivity is related to the resonance frequency shift and quality factor change, respectively, with and without sample [12]:

$$A\ (\epsilon_{1,p}-1)\ \frac{V_s}{V_c} = \frac{\omega_1-\omega_2}{\omega_1} \tag{3}$$

$$B\ \epsilon_{2,p}\frac{V_s}{V_c} = \left(\frac{1}{Q_2}-\frac{1}{Q_1}\right). \tag{4}$$

ω_1 and ω_2 are the resonance angular frequencies and Q_1 and Q_2 are the quality factors of the unloaded and loaded cavity, respectively. In consideration of the experimental setup described in section 2.2 and Figure 2,

the 'unloaded' cavity is already loaded with the quartz dewar and the empty reactor. When a sample is introduced in the reactor, the cavity is called 'loaded'. V_s and V_c are the volumes of the sample and the cavity, respectively. A and B are proportionality factors determined from calibration measurements of standard samples with known permittivity [8]. The sample under investigation must have the same shape as the reference samples and must be placed at the same position inside the cavity [12].

In order to transform the complex permittivity of the powder $\widetilde{\epsilon}_p = \epsilon_{1,p} + j\ \epsilon_{2,p}$ into the complex permittivity of the solid $\widetilde{\epsilon}_s = \epsilon_{1,s} + j\ \epsilon_{2,s}$ an effective medium theory calculation has to be applied. We used the Landau-Lifshitz-Looyenga formalism [13, 14] which is reported to provide an accurate correlation between the dielectric constants of powder and bulk in the micro- and radiowave regime for a broad range of powder volume fractions f (ratio of powder density and crystallographic (bulk) density) [15], and which gave also reliable values for semiconductor powders such as rutile TiO_2 and $SrTiO_3$:

$$\epsilon_{1,p}^{1/3} - 1 = f\left(\epsilon_{1,s}^{1/3} - 1\right) \tag{5}$$

$$\epsilon_{2,s} = \frac{\epsilon_{2,p}}{f}\left(\frac{\epsilon_{1,s}}{\epsilon_{1,p}}\right)^{2/3} \tag{6}$$

The relationship between the complex permittivity $\widetilde{\epsilon}_s$ and the complex conductivity $\widetilde{\sigma}$ is given by the following equation:

$$\widetilde{\sigma} = \sigma_1 + j\sigma_2 = \epsilon_0\ \omega\left(\epsilon_{s,2} + j\epsilon_{s,1}\right) \tag{7}$$

σ_1 describes the dielectric and/or ohmic losses (due to bound and free charge carriers, respectively) and is hence comparable with the DC conductivity, if losses not caused by free carriers can be neglected, which is a good approximation for most semiconductors [16].

In Figure 3 the complex permittivity and conductivity, as calculated with equations (3), (4), (5), (6), and (7), and reaction product concentrations (i.e. catalytic performance) of α-V_2O_5 are plotted. It has been reported that 20 vol% oxygen in inert gas above 300 °C are sufficient to fully oxidize α-V_2O_5 and remove surface defects [17]. The electrical conductivity in V_2O_5 single crystals was described by free and bound polarons, the latter being localized at vanadium sites associated with oxygen vacancies [18]. The decrease of the conductivity in the first 20 min of the experiment can thus be explained by the healing of defects. The change from oxidizing to more reducing conditions (1 vol% n-butane/20 vol% oxygen/79 vol% nitrogen) induced an increase of the conductivity, which is characteristic for an n-type semiconductor and is in agreement with literature [19, 20]. The n-type conductivity is induced from non-stoichiometries in the oxide [3]. It was proposed that oxygen vacancies are compensated by vanadium species in lower oxidation states than the stoichiometric oxidation state +5, namely +4 and +3 [21]. In an oxidizing atmosphere the conductivity of an n-type semiconductor with appropriate reactivity decreases, while it increases in reducing gases. In a common model, this effect is explained by

the creation of acceptor like surface states in the band gap due to the chemisorption of oxygen [1, 2]. These states act as traps for mobile electrons. Hence the equilibrium between surface and bulk states is changed which modifies the surface state induced band bending. A further discussion of the physics of the conductivity will be given after presenting the results of the complementary UV-VIS reference experiment.

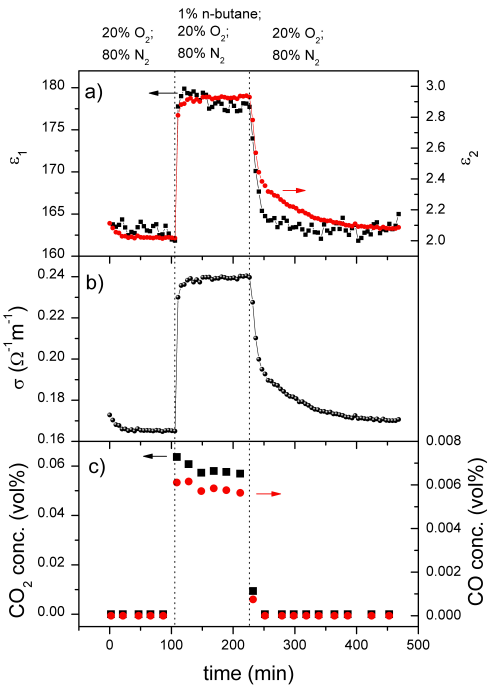

Fig. 3 a) ϵ_1, ϵ_2 and b) conductivity of α-vanadium(V) oxide in different reactive atmospheres at 400°C. c) Simultaneously measured CO and CO_2 concentrations evolved during the treatment of α-V_2O_5 in the different gas mixtures at 400 °C.

When the inital atmosphere was re-applied the conductivity decreased and approached only very slowly the value observed during the first atmosphere (Figure 3b). This is in contrast to the very fast response observed in the reducing atmosphere. Interestingly, it has been reported that the re-oxidation of vanadia catalysts is the rate-limiting step in redox reactions [2, 22, 23]. For comparison, the much more active commercial catalyst vanadyl pyrophosphate (VPP), which catalyzes the selective oxidation of n-butane to the important basic chemical maleic anhydride with high selectivities, shows very fast reduction and slow oxidation kinetics as well [10]. However, the conductivity trends in the different gas mixtures are reversed, i.e. VPP exhibts a p-type conductivity behavior. An often discussed active site in oxidation catalysts is oxygen with the formal oxidation state -1 [2]. Such an ionic surface state could be formed by the trapping of an electron hole by (surface) lattice oxygen, which might explain the often observed higher catalytic activity (and probably selectivity) of p-type semiconducting oxides (in Kröger-Vink notation):

$$h^{\cdot} + O_O^x \rightleftharpoons O_O^{\cdot} \tag{8}$$

This general statement is in agreement with other catalytically active vanadium phosphate samples investigated by the microwave conductivity technique [24].

The total value of the measured conductivity of V_2O_5 is orders of magnitudes higher than the conductivity of the selective catalyst VPP [10]. The absolute value of ϵ_2 for V_2O_5 being in the range between 2 and 3 and corresponding to a conductivity of $1.0\text{-}1.5 \cdot 10^{-1}$ $(\Omega\text{cm})^{-1}$ compares well with DC electrical conductivities of $3.7 \cdot 10^{-1}$ $(\Omega\text{m})^{-1}$

for α-V_2O_5 single crystals measured at room temperature [18], though comparisons of microwave conductivities with DC values have to be taken with care due to potentially different probed processes.

In Figure 3a the experimentally determined values of ϵ_1 and ϵ_2 are shown. As a result, both values increase similarly to the conductivity due to the change from oxidizing (20 vol% oxygen/80 vol% nitrogen) to reducing (1 vol% n-butane/20 vol%oxygen/79 vol% nitrogen) conditions and decrease when the oxidizing conditions are reapplied. This is not surprising for ϵ_2, since it is proportional to σ_1 after equation (7). The absolute value of ϵ_1 is in the range of 10^2, which compares well with values of 40 (b-axis) and 300 (c-axis) of single crystals measured at 10 kHz and about 200 K [25]. As for the catalytic reactivity, the parallel formation of CO and CO_2 indicates that the following combustion reactions took place at the surface of the catalyst:

$$C_4H_{10} + 6.5\ O_2 \longrightarrow 4\ CO_2 + 5\ H_2O \quad (9)$$

$$C_4H_{10} + 4.5\ O_2 \longrightarrow 4\ CO + 5\ H_2O \quad (10)$$

The maximum n-butane conversion was 8%. In detail, the time-dependent response of ϵ_1 and ϵ_2 show slight differences, in particular at the beginning and upon changing from the second to the third treatment. In the latter case ϵ_1 does not show the pronounced slow increase at the beginning and slow decline of σ at the end of the measurement cycle, but resembles the more rapid response of the CO and CO_2 concentration and hence the catalytic response measured simultaneously during the microwave conductivity measurement (Figure 3c). In particular the parallel decrease at the beginning of the treatment in 1 vol% n-butane/20 vol% oxygen/79 vol% nitrogen is striking. This might point to a contribution of strong surface dipoles to ϵ_1 due to the adsorption of n-butane, CO_x and reaction intermediates on the surface. Moreover, the rapid stop of the reaction after switching off the n-butane gas does correlate with ϵ_1 but not with the conductivity change. Obviously, two processes are defining the re-oxidation behavior of the catalyst, indicated by a very fast and an underlying slow decay of the conductivty. This might point to a fast surface process (coinciding with the surface-sensitive catalytic activity and ϵ_1) and a slow bulk transformation, which will be examined by complementary experimental techniques presented in the next chapters.

3.2 In situ XRPD

In order to find a possible correlation between the conductivity and permittivity dynamics in oxidizing and reducing atmospheres and a possible phase transformation or a perturbation of the lattice due to the removal of oxygen from the bulk, in situ XRPD was performed. In Figure 4a the diffractograms measured under reactive conditions (oxidizing, reaction/reducing, oxidizing conditions) are shown. In all patterns all diffraction peaks can be assigned to α-V_2O_5. In comparison to the diffractogram in Figure 1 measured at room temperature the

peaks are slightly shifted due to the anisotropic thermal expansion of α-vanadium(V) oxide [26]. However, the lattice parameters of the orthorhombic unit cell shown in figure 4b are indistinguishable in the different gas atmospheres. Hence the (major) increase of the conductivity in the 1 vol% n-butane/20 vol% oxygen/79 vol% nitrogen mixture cannot be assigned to a bulk phase transformation since no crystalline reduced phases such as V_4O_9 or V_6O_{13} have ben formed during the treatment.

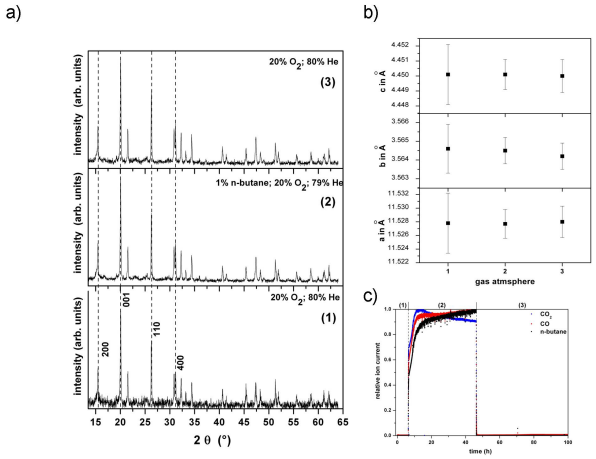

Fig. 4 In situ XRPD pattern (a), lattice parameters (b), and mass spectrometer data of CO, CO_2, and n-butane (c) evolved during the in situ XRPD measurement of the orthorhombic α-V_2O_5 powder in (1) 20 vol% oxygen/80 vol% helium, (2) 1 vol% n-butane/20 vol% oxygen/80 vol% helium, and (3) 20 vol% oxygen/80 vol% helium at 400°C.

Furthermore, in Figure 4c the ion currents (normalized to their intensity maximum) of CO (mass 28), CO_2 (mass 44), and n-butane (mass 43) recorded during the in situ XRPD experiment are shown. Upon adding 1 vol% n-butane to the 20 vol% oxygen atmosphere, the evolution of CO and CO_2 was clearly detected indicating the catalytic activity of α-V_2O_5 under the applied experimental conditions.

3.3 In situ UV-VIS

The in situ UV-VIS experiment was performed to find indications for the presence of bulk point defects and electronic states in the band gap of α-V_2O_5 due to the proposed removal of (surface) lattice oxygen [3] that can explain the observed dynamic conductivity under different reaction conditions. In Figure 5a three UV-VIS spectra are shown, each recorded after 1 hour in 20 vol% oxygen/80 vol% helium, 1 vol% n-butane/20 vol% oxygen/79 vol% helium, and again 20 vol% oxygen/80 vol% helium, respectively. The evolution of CO_2 during the treatment in the second mixture proved that the catalyst was working (not shown). α-V_2O_5 is characterized by an indirect optical bandgap [27]. Therefore, $(K/S\ h\nu)^{1/2}$ was plotted versus $h\nu$ and the band gap energy was determined by linear extrapolation of the low energy absorption edge as denoted in Figure 5a. We found a value of 1.93 eV for the band gap, which is smaller than 2.2 eV reported in literature [27]. However, it is well known that the band gap of a semiconductor decreases with increasing temperature [28]. Additionally, diffuse reflection spectroscopy systematically underestimates the band gap for crystal sizes smaller than ca. 10 μm [29]. Thus, all features at photon energies smaller than 1.93 eV are assigned to band gap states. It can be

seen that the K/S value is increased below 1.93 eV in 1 vol% n-butane/20 vol% oxygen/79 vol% helium compared to the K/S value measured in the 20 vol% oxygen/80 vol% helium atmosphere. It was reported that α-V_2O_5 single crystals exhibit absorption maxima at approximately 1.25 and 1.55 eV [19, 30, 21]. The increase of the 1.55 eV absorption observed under reducing conditions was assigned to electrons in vanadyl oxygen vacancies V_O (doubly ionizable donors) caused by the homogeneous loss of lattice oxygen without the formation of lower oxides. In the Kröger-Vink notation this can be expressed by the following formulae:

$$O_O^x \rightleftharpoons V_O^x + 1/2O_2 \tag{11}$$

$$V_O^x \rightleftharpoons V_O^{\cdot} + e' \rightleftharpoons V_O^{\cdot\cdot} + 2e' \tag{12}$$

From electron paramagnetic resonance spectroscopy results it was concluded that one excess electron in the vacancy can interact with (i.e. is localized at) empty 3d-orbitals of adjacent vanadium atoms [21]. Moreover, the rather strong near-infrared (NIR) absorption was explained by charge transfer from the localized $3d^1$ (V^{4+}) states in the forbidden band gap to the conduction band or neighboring V orbitals. Consequently, we assign the increase of K/S in this range to the presence of oxygen vacancies and adjacent vanadium(IV) states perfectly rationalizing the increased conductivity. Moreover, this is in agreement with UV and X-ray photoelectron studies showing that an occupied vanadium(IV) state appears in the bandgap of α-V_2O_5 due to the removal of lattice oxygen under reducing conditions [17, 31].

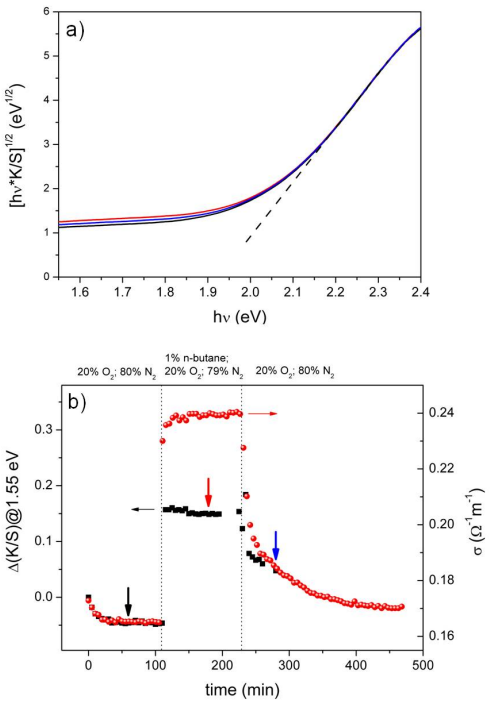

Fig. 5 (a) In situ UV-VIS spectra of α-V_2O_5 at 400°C measured after 1 hour in 20 vol% oxygen/80 vol% helium (black curve), 1 hour in 1 vol% n-butane/20 vol% oxygen/79 vol% helium (red), and 1 hour in 20 vol% oxygen/80 vol% helium (blue), respectively, as indicated by upright arrows in b), and extrapolation line of the band gap determination (broken line). (b) Absorption difference at 1.55 eV of α-V_2O_5 at 400°C during the different treatments compared to the first measured spectrum at 0 min (black squares). For comparison, the microwave conductivity measured under same conditions is shown (red circles).

When the 20 vol% oxygen/80 vol% helium was reapplied, K/S decreased again but did not reach the value of the first condition. If the absorption difference at 1.55 eV

relative to the first measured spectrum at 0 min is plotted versus time and directly compared to the conductivity response (Figure 5b) a remarkable agreement is achieved. The decrease of both absorption and conductivity at the beginning, the fast increase upon changing to reducing conditions, and the slowly falling values after re-applying the oxidizing atmosphere strongly indicate that the conductivity kinetics is governed by the (fast) formation and (slow) filling of oxygen vacancies, respectively. The latter process might be delayed due to the removal of OH groups and water molecules in the vacancies produced during the alkane oxidation reaction. However, the maximum conductivity amplitude and the kinetic trend at the beginning of the treatment in the n-butane/oxygen gas mixture, as well as the initial fast decrease at the beginning of the third treatment differ from the relative time-resolved NIR absorption, but resemble more the fast response of the catalytic activity (Figure 3c) and of ϵ_1 (Figure 3a). Since the catalytic performance is associated with surface processes, e.g. formation of adsorbates, we suggest that chemisorbed reactant, intermediate and product molecules and/or active catalytic sites on the surface, very likely changing the work function of the surface due to their dipole moments (as also indicated by ϵ_1), are contributing to the observed conductivity under reaction conditions as well.

4 Conclusions

α-V_2O_5 powder was investigated at 400°C under reactive oxidation and reduction conditions with the in situ microwave cavity perturbation technique. As a result, we observed an increase of the micowave conductivity of V_2O_5 in the presence of a reducing agent (n-butane) in the gas feed, which is characteristic for an n-type semiconductor. Moreover, in the in situ X-ray powder diffraction experiment no phase transformation or any change of the lattice parameters were observed under reaction conditions. Hence we conclude that the bulk crystal phase is stable under the applied conditions. However, in an in situ UV-VIS reference experiment the optical absorption of α-V_2O_5 increased below the (theoretical) band gap energy in the n-butane/oxygen atmosphere, which can be attributed to the formation of oxygen vacancy point defects. Due to the perfect agreement between the time-dependent response of the absorption at 1.55 eV and the conductivity under oxidizing conditions an unambiguous correlation between the formation of point defects (and V3d band gap states) and the conductivity has been proven. Since under n-butane/oxygen conditions the absolute conductivity amplitude cannot be explained by oxygen vacancy formation alone, and since the difference correlates better with the CO/CO_2 formation, we assign this contribution to surface processes such as chemisorption. Thus, these results are suggesting the enormous potential of the microwave cavity

perturbation technique for identifying and distinguishing surface and bulk processes and for elucidating their relevance for catalysis.

Acknowledgments

The authors thank Prof. R. Stößer (HU Berlin) for his continuing support of our microwave activities. Financial support by the German Federal Ministry of Education and Research (BMBF) within the framework of the ReAlSelOx project (Fkz 033R028) and by the Deutsche Forschungsgemeinschaft (DFG) are gratefully acknowledged.

References

1. T. A. Goodwin and P. Mark, Prog. Surf. Sci. **1**, 1 (1971).
2. S. R. Morrison, *The chemical physics of surfaces* (Plenum Press, 1977).
3. J. Haber, Catal. Today **142**, 100 (2009).
4. F. Cavani, Catal. Today **157**, 8 (2010).
5. N. Ballarini, F. Cavani, C. Cortelli, S. Ligi, F. Pierelli, F. Trifiro, C. Fumagalli, G. Mazzoni, and T. Monti, Top. Catal. **38**, 147 (2006).
6. R. Schlögl, Top. Catal. **54**, 627 (2011).
7. M. S. Sze and K. K. Ng, *Physics of Semiconductor Devices* (Wiley Interscience, 2007), chap. Metal semiconductor contacts.
8. M. Eichelbaum, R. Stößer, A. Karpov, C. K. Dobner, F. Rosowski, A. Trunschke, and R. Schlögl, Phys. Chem. Chem. Phys. **14**, 1302 (2012).
9. G. Fischerauer, M. Spörl, A. Gollwitzer, M. Wedemann, and R. Moos, Frequenz **62**, 180 (2008).
10. M. Eichelbaum, M. Hävecker, C. Heine, A. Karpov, C.-K. Dobner, F. Rosowski, A. Trunschke, and R. Schlögl, Angew. Chem. Int. Ed. **51**, 6246 (2012).
11. P. Kubelka and F. Munk, Z. Tech. Phys. **12**, 593 (1931).
12. L. Chen, C. Ong, C. Neo, V. Varadan, and V. Varadan, *Microwave Electronics: Measurement and Materials Characterization* (Wiley, 2004).
13. L. D. Landau and E. M. Lifshitz, *Electrodynamics of continuous media* (Pergamon Press, 1960).
14. H. Looyenga, Physica **31**, 401 (1965).
15. D. C. Dube, J. Phys. D: Appl. Phys. **3**, 1648 (1970).
16. W. Bauhofer, J. Phys. E: Sci. Instrum. **14**, 934 (1981).
17. M. Heber and W. Gränert, J. Phys. Chem. B **104**, 5288 (2000).
18. C. Sanchez, M. Henry, J. C. Grenet, and J. Livage, J. Phys. C Solid State Phys. **15**, 7133 (1982).
19. N. Kenny, C. Kannewurf, and D. Whitmore, J. Phys. Chem. Solids **27**, 1237 (1966).
20. V. A. Ioffe and I. B. Patrina, Phys. Status Solidi B **40**, 389 (1970).
21. L. Fiermans, P. Clauws, W. Lambrecht, L. Vandenbroucke, and J. Vennik, Phys. Status Solidi A **59**,

485 (1980).

22. H. Clark and D. Berets, in *Proceedings of the International Congress on Catalysis*, edited by A. Farkas (Academic Press, 1957), vol. 9 of *Advances in Catalysis*, pp. 204 – 214.
23. G. Simard, J. Steger, R. Arnott, and L. Siegel, Ind. Eng. Chem. **47**, 1424 (1955).
24. M. Eichelbaum, R. Glaum, M. Hävecker, K. Wittich, C. Heine, H. Schwarz, C.-K. Dobner, C. Welker-Nieuwoudt, A. Trunschke, and R. Schlögl, ChemCatChem **5**, DOI: 10.1002/cctc.201200953 (2013).
25. W. M. Haynes, ed., *CRC Handbook of Chemistry and Physics* (CRC Press, 2012), 93rd ed.
26. I. Corvin and L. Cartz, J. Am. Ceram. Soc. **48**, 328 (1965).
27. C. Q. Granqvist, ed., *Handbook of Inorganic Electrochromic Materials* (Elsevier Science B.V., 2002).
28. Y. P. Varshni, Physica **34**, 149 (1967).
29. W. N. Delgass, G. L. Haller, R. Kellerman, and J. H. Lunsford, *Spectroscopy in Heterogeneous Catalysis* (Academic Press, New York, 1979).
30. P. Clauws and J. Vennik, Phys. Status Solidi B **66**, 553 (1974).
31. Q.-H. Wu, A. Thissen, W. Jaegermann, and M. Liu, Appl. Surf. Sci. **236**, 473 (2004).